

Alternative screening method for analyzing the water samples through an electrical microfluidics chip with classical microbiological assay comparison of *P. aeruginosa*



Ismail Bilican^{a,b}, Tolga Bahadir^c, Kemal Bilgin^d, Mustafa Tahsin Guler^{b,e,*}

^a Science and Technology Application and Research Center, Aksaray University, Aksaray, 68100, Turkey

^b UNAM—National Nanotechnology Research Center, Institute of Materials Science and Nanotechnology, Bilkent University, 06800, Ankara, Turkey

^c Department of Environmental Engineering, Faculty of Engineering, Aksaray University, Aksaray, 68100, Turkey

^d Department of Medical Microbiology, Medical School, Ondokuz Mayıs University, Samsun, 55139, Turkey

^e Department of Physics, Faculty of Art and Science, Kirikkale University, Kirikkale, 71450, Turkey

ARTICLE INFO

Keywords:

Microfluidic chip
Electrical detection
P. aeruginosa
Bacteria
Water analysis

ABSTRACT

Pseudomonas aeruginosa is a pathogenic bacterium in fresh water supplies that creates a risk for public health. Microbiological analysis of drinking water samples is time consuming and requires qualified personnel. Here we offer a screening system for rapid analysis of spring water that has the potential to be turned into a point-of-need system by means of simple mechanism. The test, which takes 1 h to complete, electrically interrogates the particles through a microfluidic chip suspended in the water sample. We tested the platform using water samples with micro beads and water samples spiked with *P. aeruginosa* at various concentrations. The mono disperse micro beads were used to evaluate the performance of the system. The results were verified by the gold standard membrane filtration method, which yielded a positive test result only for the *P. aeruginosa* spiked samples. Detection of 0–11 k bacteria in 30 μ L samples was successfully completed in 1 h and compared with a conventional microbiological method. The presented method is a good candidate for a rapid, on-site, screening test that can result in a significant reduction in cost and analysis time compared to microbiological analyses routinely used in practice.

1. Introduction

The first micro-machined electrical microfluidic chip was produced by Ayliffe et al. [1]. Using an impedimetric technique, the identification and detection of several cells are shown in published literature, such as CD4 T-cells [2], general blood cells [3], yeast cells [4], stem cells [5], lymphocytes [6] and leukemia cells [7]. Applications of the technique are not limited to cell measurement. So far, detection of circulating exosomes [8], droplet speed and size measurement [9], as well as the detection of metal wear particles inside engine oils have been shown [10].

Waterborne infections pose a significant threat to populations across the world, especially in developing and under-developed regions [11]. The gold standard microbiological cultivation methods lack of swiftness means it can take up to a few days or even weeks to verify the pathogenic contamination from environmental or clinical samples [12]. Therefore, as a highly sensitive and fast technique, electrical microfluidic applications can be used for detection of pathogens to address

the speed and cost issues.

Impedimetric bacteria detection inside microchannels was first realized by Bernabini et al. by using oil to focus the suspending solution from the two sides towards the middle of the channel in the sensing region, which consists of top and bottom electrodes [13]. Since the bacteria are nearly 20 to 30 times smaller than RBC in volume, the acquired signal from the bacteria is very low. Hydrodynamic focusing of the conductive suspending solution with an insulating oil leads to a restriction of electric field lines and enhances the sensitivity that enables detection. However, hydrodynamic focusing requires very fine tuning of flow rates that cannot be achieved with simple pumping technique. Besides, the surfactant needs to be dissolved inside the oil to get a continuous water-oil flow that increases the complexity and cost. Haandbaek et al. succeeded in the detection of *E. coli* and *B. subtilis* at very high excitation frequencies that employed RC resonance consisting of inductors connected to the top and bottom electrodes to improve the sensitivity [14]. In their setup, the incoming particles were focused into the middle of the channel by DEP (dielectrophoresis) through

* Corresponding author. Department of Physics, Faculty of Art and Science, Kirikkale University, Kirikkale, 71450, Turkey
E-mail address: gulermt@kku.edu.tr (M.T. Guler).

additional micro electrodes integrated within the chip. Since the bacteria are very small and produce a very low signal magnitude, opacity – which is the ratio of high to low frequency impedance [15] – is inadequate to distinguish between the bacteria and beads, which is the main drawback of electrical systems. Selectivity of the impedimetric devices can be done through immobilization of bio-molecules – which have an affinity to the analyte – around the sensing region. Upon binding of the target particle, the impedance changes due to blockage of the electric current. Antibodies [16], aptamers [17], peptides [18], and antibody-coated nanoparticles [19] are among the selective molecules that are immobilized in the sensing region.

Detection of pathogens in liquid samples is one of the main topics of interest to the LOC community. The μ TAS (Micro total analyzing system) with integrated microfluidic channels and fluid control units allow a system that is of comparable size to the particles of interest [20,21]. Microfluidic chips enable rapid detection of bacteria using various other techniques like optical [22,23], electrochemical [24,25], surface plasmon resonance (SPR) [26], quartz crystal microbalance (QCM) [27] and cantilever sensors [28]. Optical detection techniques are the most similar ones among the other techniques with regards to their detection principle. The only drawback is the requirement to integrate some optical components like optical fibers, lenses, laser sources, photomultiplier tubes, CMOS sensors, etc. [29–31]. The electrochemical technique is the Faradaic versions of the impedimetric one that measures the current generated by oxidation or reduction of specific chemical materials inside the solution. By functionalizing the electrode surfaces, the chemical reaction occurs in the presence of the analyte around the electrode detecting the bacteria as shown in published literature with numerous versions of micro devices [32]. Whilst its electrode and microchannel design slightly differs from the impedimetric one, using labeled molecules is a necessity, as well as using a redox catalyst. The SPR measurement principle is based on sensing the variation in the angle of reflected light upon changing the optical properties of the medium. Thus, it requires surface functionalization [33] with a complex optical setup for analysis. Whilst being sensitive and selective, it requires expensive bio-molecules in addition to precision optical instruments. QCM measures the change in the resonant frequency of quartz crystals because of the mass alteration induced by binding the pathogens onto the surface. Fabrication is carried out with double-sided electrode formation on a pure quartz crystal substrate, which makes it an expensive device in comparison to an impedimetric detection chip. In addition, it needs surface functionalization with antibodies [34]. A cantilever sensor is also a very tiny device that is hard to engineer. A cantilever sensor measures the deflection of a reflected laser beam from the surface upon binding of the analyte [35]. Utilizing this technique for bacteria detection needs a functionalized cantilever surface as well as an advanced optical setup, which make it hard to use. There are also molecular biological techniques like polymerase chain reaction (PCR) [36] and loop mediated isothermal amplification (LAMP) [37] that have been adapted to LOC systems for detection of pathogens. Several versions of LOC PCR [36,38] and LAMP [37] systems developed for pathogen detection can be found in published literature. These are the ultimate detection techniques targeting the species-specific genetic sequences and generate millions of this DNA sequence through nucleic acid reactions for fluorescent detection. On the other hand, these techniques need previous cell lysis to reveal the genetic material. The lysate is processed with several biochemical substances at specific temperatures to increase the number of DNA sequences that is further fluorescently tagged. These protocols require integration of many environmental gadgets to the microfluidic chip, including valves, temperature sensors, heaters, etc. Fabrication of such a device is hard and expensive in comparison to ours.

In this study, we have reported on an electrical microfluidic system consisting of coplanar measurement electrodes and microchannels, which are very easy to fabricate and integrate, unlike the top and bottom electrodes that require very precise alignment. In addition, our

system does not require any previous focusing of the sample to be able to detect particles of the size of bacteria. A two-stage filtering mechanism prevents clogging that enables working with very narrow channels to achieve high sensitivity as well as simplicity. Though bio-molecules like antibodies or nucleic acids provide selectivity for a test, those reagents have to be replaced every time before running a new test. Hence, by giving up selectivity, our system provides down to single-particle sensitivity in 30 min with a cost-effective, multiple use, microfluidic chip for preliminary screening of water samples. The accuracy of our method is tested with blank, micro bead and *P. aeruginosa* spiked samples by comparing it to the output of a membrane filtration analysis using the same samples.

2. Materials and methods

In this study, we fabricated a microfluidic chip consisting of polydimethylsiloxane (PDMS) microchannels and gold microelectrodes. The microelectrodes were connected to a lock-in amplifier for electrical detection. The water sample was spiked with *P. aeruginosa* or mono disperse polystyrene (PS) micro beads (Polysciences, Inc.), and some phosphate buffer saline solution (PBS, $10 \times$, 7.4 pH –Thermo Scientific, ABD) was added to the water in a 15.6% v/v ratio to get conductivity of 2.5 S/m. The spiked water samples were filtered using a syringe filter (Millipore) with a pore size of 5.6 μ m before pumping to the microchannel. Then, a 30 μ L test sample was run through the microfluidic chip while performing real-time electrical measurements. As the particles were passing over the electrodes an impedance peak was observed for every single particle due to blockage of the electric current. Then, a 30 μ L specimen was taken from the same sample and sent to a microbiology lab to compare with a membrane filtration analysis.

2.1. Mold fabrication

A schematic representation of the channel mold fabrication is shown in Fig. S1. A four-inch diameter silicon wafer is washed with acetone, isopropyl alcohol (Sigma Aldrich) and DI water, then dried with nitrogen flux. The wafer is baked at 110 °C for 10 min to allow the evaporation of every solvent molecule remaining on the surface. SU8 2005 (MicroChem), a negative photoresist (PR), was poured over the wafer directly from the bottle to cover a circle with dimensions half the diameter of the wafer. The first layer of PR is coated for better adhesion to the active second layer. Hence, after spin coating and heat treatment, UV is applied without a mask. The second layer is spin coated at 850 rpm for 35 s (Fig. S1b). After heat treatment to harden the PR at 65, 95 and 65 °C for 3, 6 and 2 min, respectively, UV exposure is applied using a mask aligner (EVG620) through a glass/chromium photomask (Fig. S1c). The mask design was prepared using Layout Editor and the mask fabricated using a laser scanning mask writer (Heidelberg Instruments DWL-66). After UV exposure, the SU8-coated wafer was dipped into developer (MicroChem) for 1 min to obtain the desired microchannel pattern (Fig. S1d). In order to prevent the SU8 coming away from the wafer during the PDMS is peeled off after curing, some epoxy resin is brushed to the edge of the wafer to stick the PR layer to the wafer.

PDMS (Dow Corning Sylgard 187) is mixed with its curing agent at a weight ratio of 1:10. After thorough mixing, it is put in a vacuum chamber to release the bubbles from the mixture, which takes nearly 30 min. Then the mixture is poured onto the mold and placed on a hot plate for 2 h at 100 °C. The PDMS is cured and hardened by the heat to take the shape of the mold and then it is peeled off. Hence the pattern on the mold is transferred to the PDMS where all the extrusions on the mold form the microchannels in the PDMS slab. SEM images of the PDMS microchannels are shown in Fig. 1, which are the microchannels used for *P. aeruginosa* detection, and have dimensions of 10 μ m in height and 30 μ m in width.

Fig. 1a shows the top view of the microchannel inlet, where square-shaped staggered filters are present to avoid clogging of the

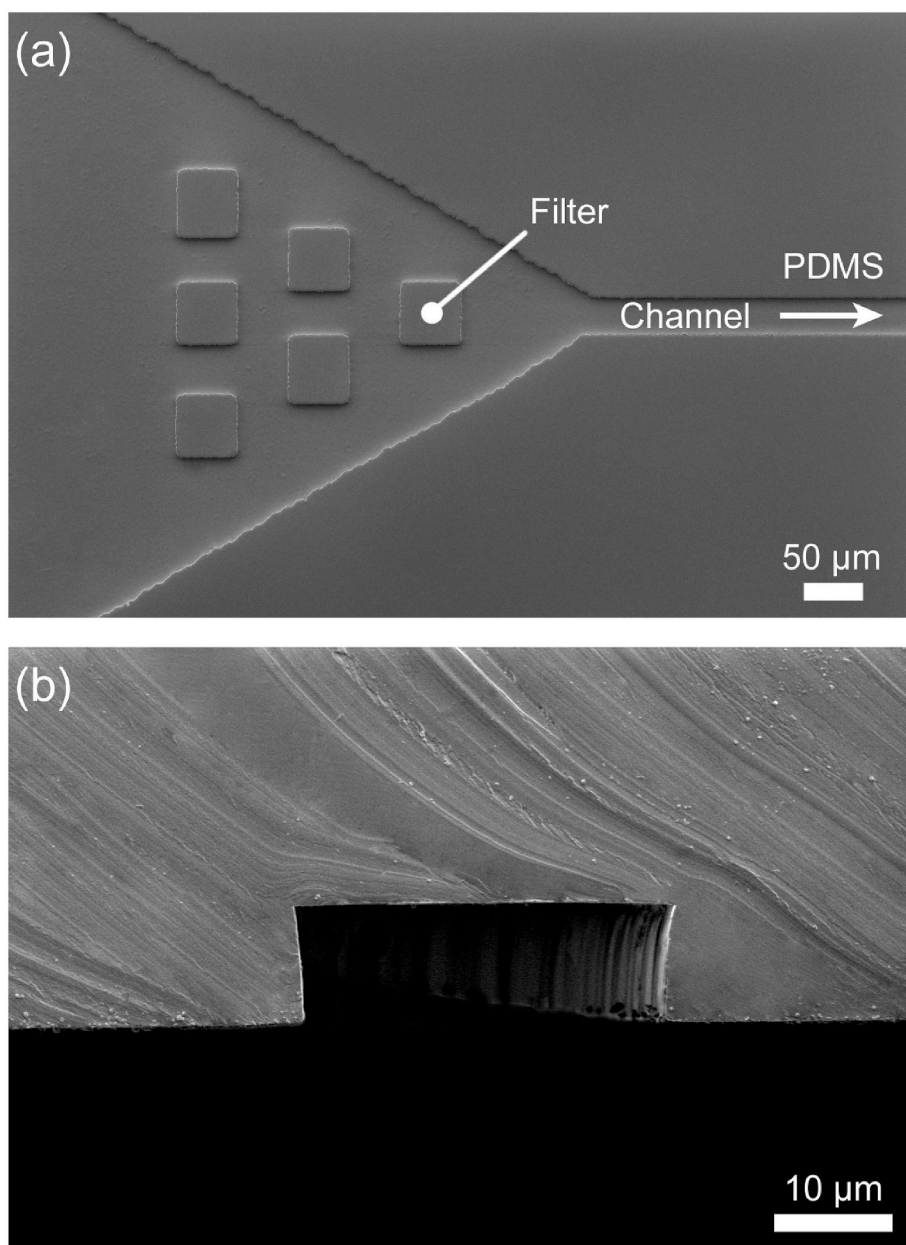


Fig. 1. SEM images of PDMS microchannels (a) top-view of the channel inlet with filtration section (b) cross-sectional image of the main microchannel.

microchannel by large-scale particles. The $50 \times 50 \mu\text{m}$ squares are drawn on the mask of the microchannel during the design step, which are implemented as pillars on the PDMS replica of the mold.

2.2. Electrode fabrication

The next step in the microfluidics chip fabrication was manufacturing the microelectrodes. These are created with a lift-off process to finish the fabrication of $10 \mu\text{m}$ -wide gold microelectrodes. A mask was designed and produced as mentioned above in the microchannel fabrication step. A standard cleaning process was applied to the glass slide in the sonicator bath by dipping the substrate glass slide in acetone, methanol and isopropyl alcohol (Sigma Aldrich) for 1 min, and a DI water flush and nitrogen drying were applied to the glass slide after each step. HMDS (Hexamethyldisilazane) and AZ5214 (MicroChem) PR were spin coated onto the glass slide at 4000 rpm for 50 s and 5000 rpm for 40 s, respectively. Here the HMDS is used for better adhesion of the PR to the glass surface. After heat treatment for 1 min at 110°C on a

hotplate, the glass slide was placed on the mask aligner and exposed to UV at $40 \text{ mJ}/\text{cm}^2$ and followed by a developer step. This time the UV exposed areas were peeled off, since the AZ5214 is a positive PR. The metallization process was performed by thermal evaporation of 15 nm chromium and 50 nm gold in a thermal evaporator (VAKSIS, MIDAS PVD 3T). Molybdenum and tungsten boats were used for gold and chromium evaporation, respectively. The physical vapor deposition process was carried out at vacuum pressure of 10^{-6} Torr. In order to achieve uniformity, the deposition was realized at a relatively slow rate, which was 0.05 nm/s at a 40 A and 80 A current magnitude (60% and 30% power rate) for gold and chromium, respectively. The metal-coated glass slide was put in acetone which etched the remaining PR on the glass slide. Hence, the metal layer sitting on the PR is also peeled off which forms the metal electrodes. Only the metal layer directly deposited on the glass surface remained on the glass slide. A simple representation of electrode fabrication process is shown in Fig. 2.

The last step of the fabrication is bonding of the microchannel and the microelectrodes. We used nuts and bolts to reversibly bond the two

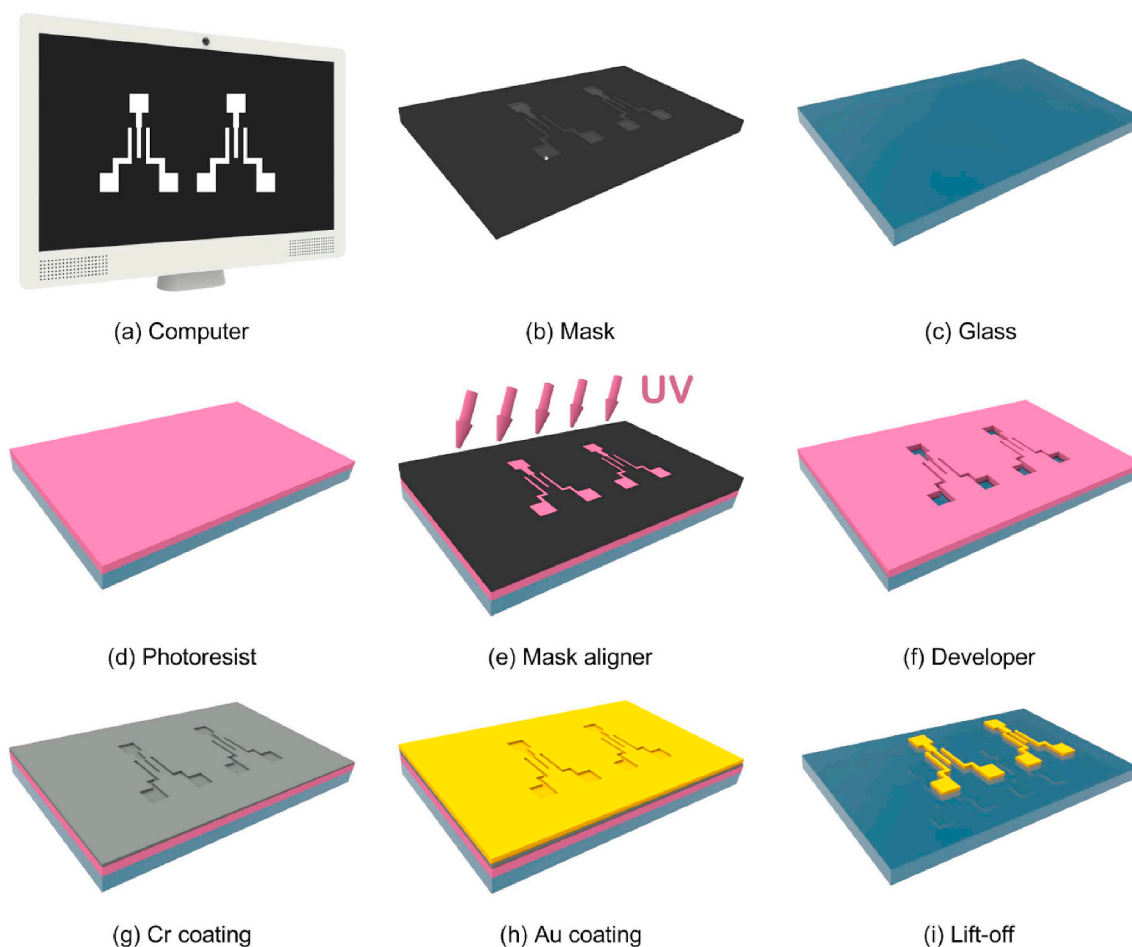


Fig. 2. Schematics of the electrode fabrication process (a) the mask is designed by computer (b) printed with a mask writer over chromium-coated soda lime glass (c) glass slide is cleaned (d) PR is spin coated over the glass slide (e) UV exposure is delivered via the mask aligner (f) the glass slide is dipped in developer solution that etches the UV-exposed PR (g) 15 nm chromium is coated in the first step, (h) a 50 nm gold layer is coated in the second step in a thermal evaporator (i) the glass slide is dipped into acetone to etch the PR and everything above it leaving the gold micro electrodes on the glass surface. (For interpretation of the references to color in this figure legend, the reader is referred to the Web version of this article.)

pieces, The PDMS microchannel and glass slide was sandwiched between two laser-cut Plexiglas parts fixed with nuts and bolts. Windows corresponding to the inlet, outlet holes, the channel and the contact pads were carved out from the upper part of the Plexiglas. A photograph of our microfluidics chip is shown in Fig S2.

2.3. Experimental set-up

Our experimental setup consisted of a lock-in amplifier (HF2LI - Zurich Instruments) that was connected to the microfluidics chip via coaxial cables as well as a pressure pump (Elveflow – OB1) connected to the vials containing the sample. The samples are sent through the microchannel by connecting the vials output tubing (Cole-Parmer 95702) to the channel inlet via a flat metal syringe tip. The pressure value is set from the pump's user interface (UI) on a PC, then the flow is started. During the electrical measurements, the samples were sent at a constant pressure of 330 mbar from the vial producing a 30 $\mu\text{L}/\text{h}$ flow rate in the microchannel used.

Using the automatic scanning feature of the lock-in amplifier, 1.5 MHz was determined to be the least noisy frequency point. Thus, the middle electrode is excited by the lock-in amplifier's interior AC signal generator at 1.5 MHz. The amplitude of the excitation voltage was set to 3 V_{p-p} to achieve the best signal to noise ratio (SNR). Comprehensive details of this were given in our previous work [7]. This signal forms a current inside the chip driving the ions inside the

solution back and forth. The output is connected to the trans-impedance amplifier (HF2TA - Zurich Instruments) from the second electrodes. The trans-impedance amplifier turns the incoming current into a voltage to be transferred to the lock-in amplifier. The lock-in amplifier analyzes the voltage using its hardware and software reducing the noise as much as possible so that it can detect tiny particles such as bacteria. A drawing that represents the measurement setup is shown in Fig. 3. Bacteria, as living cells, have a conductive cytoplasm and thin insulator membrane and are suspended in the ionic solution and flow inside the channel. When the bacteria arrive at the electrodes, the thin membrane blocks the current during transit and the current reverts back after the bacteria leave the electrode region. The fluctuating current signal is converted to a voltage in the trans-impedance amplifier and transferred to the lock-in amplifier. The lock-in amplifier processes the signal, which is monitored on the computer screen continuously where a single peak and trough occurs on the screen during the transit of the bacteria. Since there are in-phase and out-of-phase components in the output current according to the excitation voltage, the amplitude and phase data are monitored and recorded via the lock-in amplifier. The peak height is taken as the half value of the signal from peak to trough for amplitude and phase parameters. Transit time, as another parameter, is defined as the time between the peak and trough points of the signal as shown in Fig. 3. The data is recorded in CSV form that is further processed by a custom Python code employing Pandas library to handle the large amount of data together with several other libraries. As the

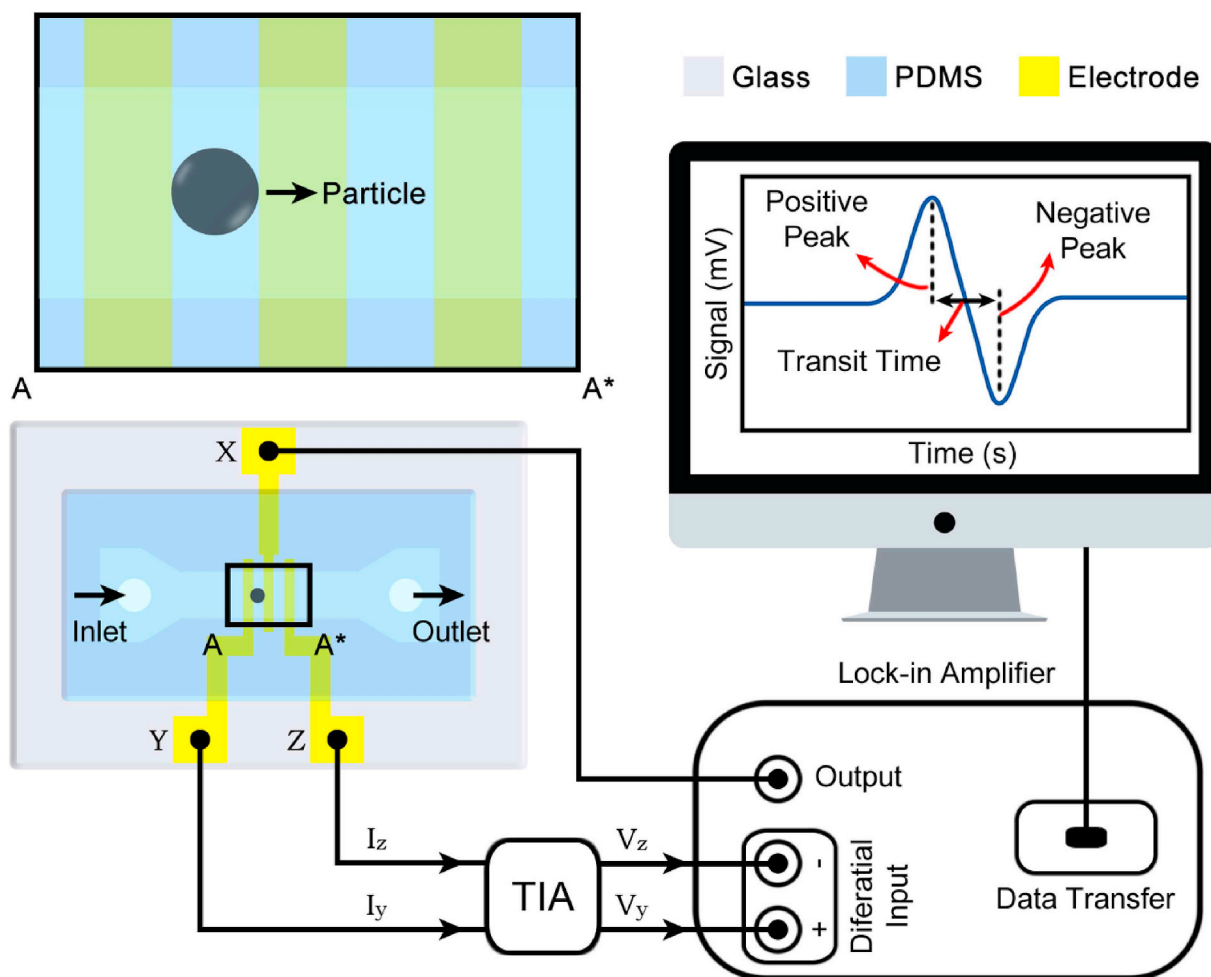


Fig. 3. A representative drawing of the experimental set-up: The middle electrode is directly connected to the lock-in amplifier's AC output. Counter electrodes are first connected to the outbox trans-impedance amplifier (TA) where the current is converted to a voltage and transferred to an inbox differential amplifier to amplify the difference between them. Assuming perfectly identical electrodes, 0 V is sent to the lock-in amplifier for the 'no particle' state. Once a particle passes through the electrodes, the balance between the current flowing via the counter electrodes are distorted and the fluctuations are detected by the lock-in amplifier, as shown in the representative monitor. Here, the peak value is calculated as half the sum of the positive and negative peak heights as well as the transit time, which is also calculated as the time interval between the positive and negative peak points.

sampling rate of the lock-in amplifier is set to 20 kHz, more than a million data points are collected after 1 min of recording, which is hard to process but good for catching details about the particles.

2.4. Detection of *P. aeruginosa* in spiked water samples using the culture method

P. aeruginosa ATCC 27853 samples were cultivated in blood agar and incubated at 37 °C overnight. After checking the purity of the *P. aeruginosa*, bacteria were transferred to a sterile physiological saline solution (0.1% NaCl). The water samples were spiked with *P. aeruginosa* at 4 different concentrations and immediately measured with both methods such that the detection experiments were started 1 h after transplanting the bacteria from the blood agar. The membrane filtration method (TS EN ISO 16266) was used as the classical method for *P. aeruginosa* analysis. For microbiological analysis, samples were filtrated on different sterile 0.45 μm membranes (Millipore) with a vacuum pump after 10 times dilution. The filters were cultivated on selective media in Cetrimide agar plates (Hypet Aqua, Diatek, Turkey) and left in an incubator at 36 ± 2 °C for 44 ± 4 h. The Petri dish was investigated by naked eye to count the bacterial colonies. Bluish and greenish areas were accepted as *P. aeruginosa* colonies, which were also investigated under 366 nm UV light where the fluorescent areas were

assumed to be *P. aeruginosa* as well. The suspected fluorescent areas were further checked with acetamide broth and King B agar selective media (MERCK, Germany). When suspicious growths in a brown/red-dish color appeared in the petri dishes, the oxidase test was performed. Two or three drops of oxidase reagent (MERCK, Germany) was added to suspicious colonies. The reaction was considered to be positive once an intense purple color developed after 10 s.

3. Results and discussion

3.1. Principles of detection

Here the purpose of the fabricated microchip is to focus the particle over the electro-active region. In the domain near the electrodes, the electric field is very strong and forms a high current density, hence, it is called the electro-active region. When a particle passes through this region, the electrical field current lines are cut inducing a variation in the output current that is fed to a trans-impedance amplifier. Since the electrodes are connected to a lock-in amplifier which applies the excitation voltage to the middle electrode and measures the current from the outer electrodes continuously, particles are detected from the signal provided by the lock-in amplifier.

Insulating substances, like PDMS and glass, were used as

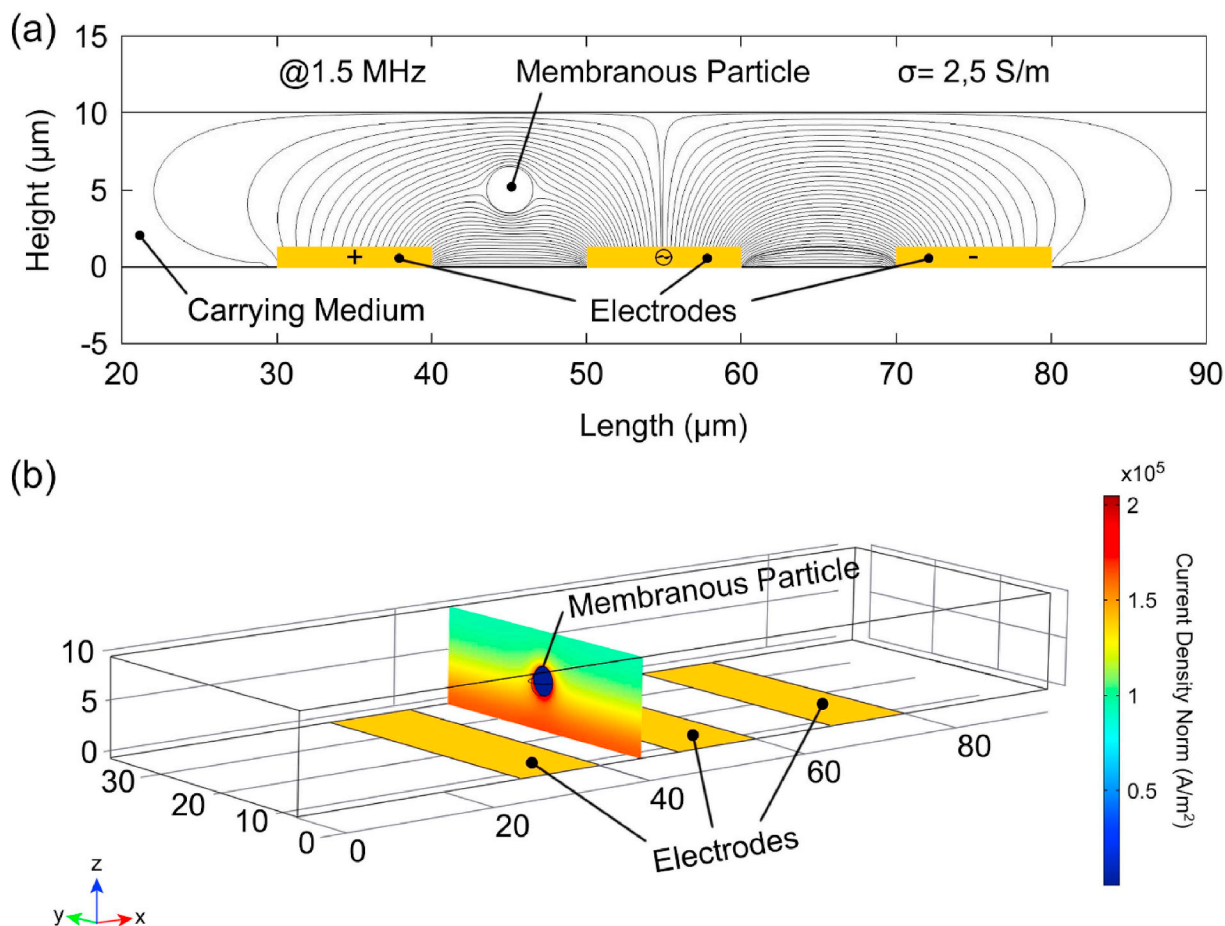


Fig. 4. The COMSOL simulation of the channel around the electrode area with a particle includes: (a) 2D simulation of the electric current stream lines which illustrates that the electrical current lines are forced to flow around the particle leading to increased impedance that can be monitored through the measurement device (b) 3D simulation of the electrical current density with cross-sectional view which shows electrical current density gradient from bottom to top generating higher current reduction for the particles passing closer to the electrodes.

microchannel material to focus the electric current lines into a narrow region so that the size of the particle becomes comparable with the electro-active region. Therefore, channel dimensions are critical in terms of the sensitivity of the measurement as shown before [7]. Lowering the channel width decreased the noise but kept the signal constant, which meant a better SNR. Furthermore, the channel height determined the distribution of the electric current lines from bottom to top as the electrodes are on one side of the channel in a coplanar design Fig. 4. Accordingly, the same size particles passing closer to the electrodes gave higher signals. To decrease this disadvantage – the biggest of the coplanar electrode design – the channel height needed to be as low as possible or the particles needed to be focused at a constant height. Since we do not want additional complexity in our chip, like hydrodynamic focusing etc., a channel height of 10 μm and channel width of 30 μm was adopted in our measurements.

A 2D and 3D COMSOL simulation of the phenomenon is shown in Fig. 4, which was produced at an excitation voltage of 1 V and a 1.5 MHz excitation frequency. Here the 2D simulation demonstrates the disruption in the electrical current field lines during the passage of the particle that leads to a reduction in the total current and increases the impedance. Fig. 4 shows a particle with an insulation membrane of 0.0001 S/m with a conductive interior of 0.6 S/m suspended in a conductive medium of 2.5 S/m, which are the corresponding parameters representing the experimental conditions. While the membrane thickness is very low, it blocks the current and increases the path length of the electric field current lines as well as the impedance. The 3D simulation shows that the current density reduces by moving away from

the electrodes and the current cannot penetrate into the particle, instead it flows around, which is shown as the reddish area around the particle as the current lines are squeezed.

The biggest challenge in pathogen detection is the small size of bacteria that induces low output signals in the detection unit and leads to a low SNR. According to the simulation results demonstrated in Fig. 4, electric current flows around the membranous particle as if the particle is a non-membranous bead, at 1.5 MHz. To achieve the maximum SNR, a frequency of 1.5 MHz was determined to carry out the measurement even though penetration of the electric current into the membrane is possible at higher frequencies. Therefore, if it had not been possible to discriminate between membranous and non-membranous particles under these conditions, it would have meant that our measurement was size sensitive and lacked the ability to discriminate bacteria from beads.

3.2. Reversible bonding and filtration

Our microchannel design is very low in height to enhance the sensitivity, which makes the channel more prone to clogging. Although there is two-stage filtering, the channels might clog due to misuse or the channel inlet filter itself may clog when frequently plugging the connector in and out. In addition, the channel inlets can also split due to harsh and intense usage that leads to leakage. When the channel is blocked or starts leaking, the whole microfluidics chip can become unusable if the bonding is irreversible, which means a waste of time and money. Therefore, plasma bonding was not employed due to its non-

reversible character, even though it is the most common method. Reversible bonding with nuts and bolts enables the PDMS channel to be separated from the glass and to be replaced with a new one or replacing the same channel after cleaning. In addition, electrode sets were made very close to each other in our design to save on space to produce as much electrode as possible in a single fabrication session in the clean room. A single channel lays on 2 electrode sets covering both electrodes. In case of channel or electrode break down, 2 electrode sets are lost at once with irreversible bonding. Hence, mobility of the micro channel permits jumping to the next electrode set once the first has deteriorated through several possible reasons such as high voltage, defective fabrication etc.

The filtration system consists of two stages, which are the syringe filter and the channel inlet filter. The latter one prevents flow of the wear remnants to the channel. Wear remnants form during the punching of the inlet and outlet holes to the PDMS microchannel. In addition, plugging the fluidic connectors in and out of the inlet holes also produces wear particles that go through the channels after the flow starts. Those wear remnants induce channel clogging as an inherent property of the PDMS channels independent from the sediments contained in the sample. On the other hand, dust particles hanging in the air may stick around the inlet when the fluidic connectors are unplugged. The dust particles are pushed through the inlet while plugging in the connectors which are carried to the channel when the flow is started that can also lead to clogging. Therefore, a self-filtered channel is the only way to prevent this type of clogging based on our experience. Moreover, the channel inlet filter falls short in filtering the smaller particles due its relatively big size. Small particles are possibly found inside the sample which requires a previous filtration stage. The best way is to filter the sample with a syringe filter before running through the channel. A filter of 5.6 μm pore size blocks anything inside the sample except for pathogens or the particles that are the same size as the pathogens. Our two-stage filtering mechanism worked very well during our experiments ensuring a smooth and continuous flow.

3.3. FEM simulation

Some FEM (Finite Element Method) simulation was performed using COMSOL(R) MULTIPHYSICS 5.0 software to compare with the experimental results. For 2 and 3 μm diameter PS beads, simulations were done using the electrical parameters from our previous work [39]. For both size beads, the particle height was arranged to give the same distance from the top and bottom of the channel to the bead's closest point. Thus, the center of the 2 μm diameter particle was assigned a range from 1.5 to 8.5 μm , and the center of the 3 μm diameter particle was assigned a range from 2 to 8 μm in 0.5 μm steps. The COMSOL simulation was run at a mesh setting with minimum and maximum element sizes of 0.01 and 1.0 μm respectively at a 1V excitation voltage and 1.5 MHz frequency; the results are given in Amperes in Fig. 5a. Here, the simulation results can explain the reason for the variation in the experimental results for the same size particles. The highest peak of the 2 μm diameter beads taking the shortest path to the electrodes gives nearly the same value as the lowest peak of the 3 μm diameter bead that takes the longest path to the electrodes. The overlapping signals of different size particles cause some difficulties in discriminating between the objects according to their size. However, the performance of the system still has the capability to distinguish 2 and 3 μm diameter particles according to the simulation results shown in Fig. 5a. The simulation shows that only the highest peak value of the 2 μm diameter bead intersects with the some of the lowest values of the 3 μm diameter beads whose routes are over 7 μm above the channel surface. With only 4 out of 28 data points intersecting, according to Fig. 5b, simple statistical calculations show this represents a 14.3% failure to distinguish between the particles based on the signal height. On the other hand, these peaks come from the lowest and highest paths of the beads inside the channel where the wall lift force is very active, which does not favor the

positions close to the channel walls and further decreases the failure number below 14.3%. This achievement arises from the relatively low channel ceiling that holds the particle in a small height range closer to the electro-active region as shown in Fig. 5b, which in turn leads to a reduction in the variation of the signal helping to discriminate between the particles.

3.4. Electrical measurements

Characterization of our device was performed with uniform 2 and 3 μm diameter mono disperse PS micro beads which were suspended in a 2.5 S/m PBS solution in different vials. The SEM pictures of the PS micro beads are given in Fig. S4. The vials were connected to a pressure pump, and the 2 and 3 μm diameter beads were sent through the microchannel separately at a constant pressure. Results of the electrical measurements are plotted in Fig. 6, which demonstrates that our system is able to distinguish between 2 and 3 μm diameter PS particles. Those results are in accordance with the simulation results discussed in the previous chapter that showed the particles with lower paths cutting more electric field current lines than the particles at higher paths. Since the heights of the particle paths inside the channels showed variations, peaks produced from the same sized particles varied as well.

In Fig. 6 three different parameters were calculated and plotted, which are the peak heights of the amplitude and phase, and the transit time, where all the 3 combinations are shown as scatter plots. Fig. 6a shows that phase and amplitude produce the same trends without giving any extra information. Transit times were in the same range for both 2 and 3 μm diameter particles that cannot therefore be used as a distinguishing parameter. Therefore, only one of the amplitude or phase parameters would be enough for size-based particle identification. The amplitude parameter was chosen for the rest of this study.

A 2.5 S/m PBS solution was spiked with *P. aeruginosa* and sent through the channel via a pressure pump to test the possibility of the electrical detection of *P. aeruginosa*. Results of the electrical measurement are shown in Fig. S5 where every single amplitude peak corresponds to a single *P. aeruginosa* bacterium. As the bacterial volume is not constant like the beads, the results show bigger variations than the bead results. A magnified view of a single peak is also shown in Fig. S5b, which represents a single bacterium. Also shown is a closer look at *P. aeruginosa* with the SEM image in Fig. S5c.

3.5. Comparison of the electrical and classical microbiological analysis

The aim of this study was to diagnose suspected water samples swiftly. While the sample cannot be classified as pathogenic or not with this on-chip electrical method, it can be diagnosed as suspect or not. After a rapid on-chip inspection, the suspected samples might be sent to labs for further analysis as to whether it is pathogenic or not, which requires finding the exact species of the cells inside the sample. To test this idea, a water sample that had been tested and confirmed free of any contamination was spiked with *P. aeruginosa* at different concentrations. The sample's conductivity was set to 2.5 S/m for electrical measurements and filtered via 5.6 μm filters to prevent channel clogging. The filter size was chosen specifically to select particles having the same size as the pathogens and prevent the passage of particles bigger than the channels, which could induce clogging and malfunctioning of the chip. The samples spiked with different concentrations of *P. aeruginosa* were sent through the channels separately and electrical measurements were performed with a lock-in amplifier. It took 1 h to test each 30 μL sample. According to the results, the water sample free of contamination did not produce any significant peaks while the other samples carrying the bacteria gave peaks that should be considered as dangerous. For comparison with the classical microbiological methods, all 5 samples were sent to a microbiology lab for testing with the membrane filtration method. The plain and bead carrier samples did not give any positive results while the spiked samples gave positive

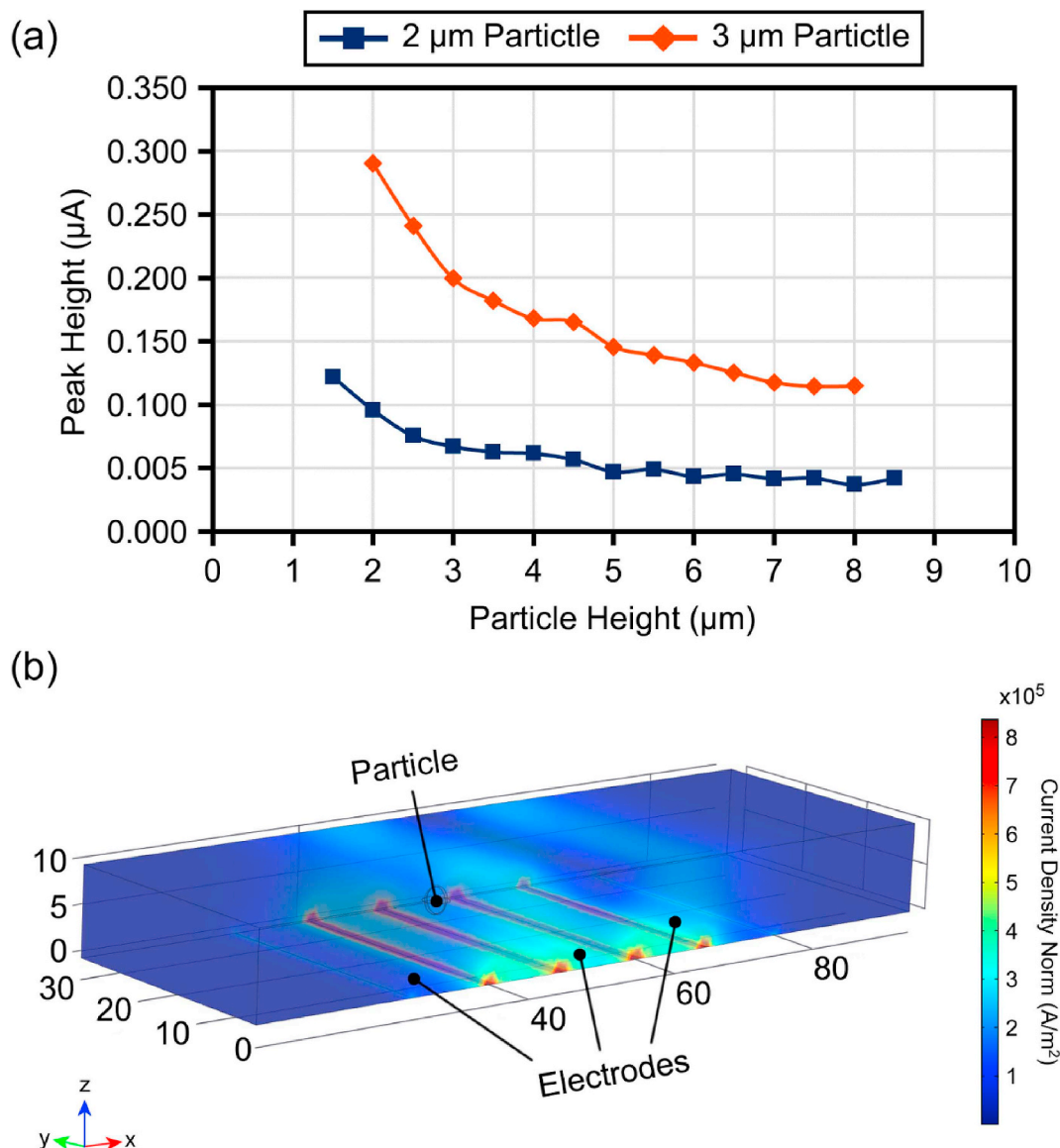


Fig. 5. FEM simulation of microfluidic chip includes: (a) Calculation of the peaks for the 2 and 3 µm diameter beads passing over the electrodes at several heights. The bigger size particle gives a higher signal as it cuts more electrical field current lines. In addition, signal reduction takes place for higher particle routes which adds complexity in distinguishing the particles with regard to size. The plot shows that signals coming from the higher paths of the 3 µm particle overlap with the signals coming from the lower paths of the 2 µm particle (b) 3D domain simulation of the electrical current density distribution indicating higher electric current density near the electrodes.

results, as shown by the photograph in Fig. 7. According to these results, the magnitude of the signal varied depending on the size and position of the particles despite the noise level being constant in all the experiments.

For the electrical measurements, the micro bead solution gave a positive result while the plain solution gave a negative result. Hence, the result for the electrical measurement of the micro beads can be called a false positive, as it gave a negative result in the gold standard microbiological analysis. In the other experiments, low concentration spiked solutions produced 3000 particles/mL for the lock-in amplifier measurement and 800 CFU/mL in the conventional assay. The medium spiked solution produced 5000 particles/mL in the electrical measurement and 1400 CFU/mL in the conventional assay. The highly contaminated solution produced 11000 particles/mL in the electrical measurement and 6000 CFU/mL in the conventional biological assay. These results validate our approach of analyzing fluid samples in 1 h to identify samples as dangerous or not. It should be noted that the micro bead solution, which is non-hazardous, is classified as dangerous by the

electrical measurement. It means that the samples having non-hazardous particles with an equivalent size as the pathogens will also be classified as dangerous in the on-chip electrical detection as false positive outputs. However, all the contaminated samples and plain sample gave consistent results with the conventional microbiological assay, which indicated the success of the method. The results of the LOC system and the conventional membrane filtration analysis were found to be in good agreement. We are offering this LOC system as a screening method that can be used for rapid, frequent, on-site testing before proceeding with the costly and time-consuming microbiological analysis for each sample.

Our method cannot identify the type of particle detected, yet it raises a red flag for potentially infectious samples that can be further scrutinized by downstream analysis. Hence, we envision the use of this system for on-site monitoring of bottled water and recreational water where currently, if a threat is detected, more detailed laboratory analyses would have to be performed. The microfluidic chip does not require trained personnel for analysis and runs on an automated system

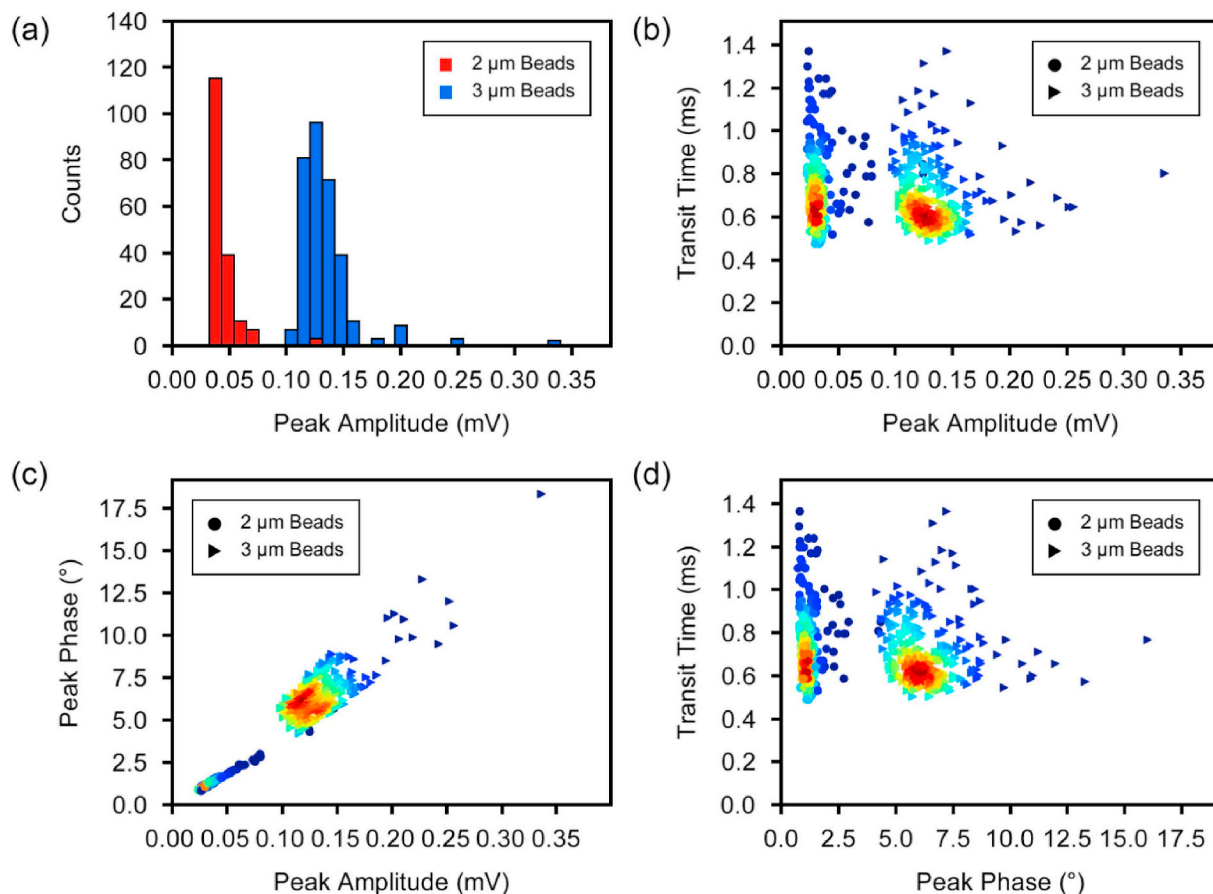


Fig. 6. Lock-in amplifier output for 2 and 3 μm diameter beads: (a) Histogram of peak amplitude (b) Scatter plot of transit time and amplitude (c) Scatter plot of amplitude and phase (d) Scatter plot of phase and transit time. Results point out that transit time is not an applicable parameter for discrimination of 2 and 3 μm diameter beads unlike amplitude and phase, which are quite good for size dependent identification.

that only needs the introduction of the sample to the microfluidic chip. The system can also be turned into a handheld analysis system by miniaturizing the electronics and plumbing components that are used in the peripheral units. This would be a very practical and low-cost testing platform solution, thanks to the small and reusable microfluidic chips introduced in this study.

All the five cases shown in Fig. 7 normally go to the lab for testing with the membrane filtration method as standard. Our method comes into play at this point removing the requirement for some tests giving no peak to be sent to the lab for standard analysis, such as the one given in Fig. 7a. Elimination of some samples for detailed analysis reduces the cost and time dramatically, since the membrane filtration method is a relatively expensive and complex method that needs clean environments and educated staff.

3.6. Miniaturization and integration

The use of this device in the field as a point-of-need tool can be possible through miniaturization of the environmental components. Our experimental setup included a PC controlled lock-in amplifier and pressure pump for both measurement and driving the samples throughout the microchannel. These are all heavy and large pieces of equipment that are hard to carry for an operator or an end user in the field. However, the μTAS community has developed many devices that can take place of the desktop tools including: a handheld custom made lock-in amplifier used for blood coagulation measurement [40], qPCR [41], on-chip active and passive pumps used for Prothrombin time measurement [42], droplet generation [43], drug analysis [44] and delivery [45]. An external battery can be used for a power source [46];

however, the best solution is to use a cell phone which offers display and computational abilities as well as power, which finds applications in several fields such as *E. coli* detection via quantum dots [47], electrochemical analysis of proteins [48] and bio-molecule detection with SPR [49]. Therefore, our setup can be miniaturized to a handheld device for fast and cost effective point-of-need analysis of water samples.

4. Conclusions

In classical microbiological methods, which are labor intensive, expensive and time consuming, all 5 samples – two of which were plain water and a PS bead suspension while the other three were spiked with *P. aeruginosa* bacteria – underwent the same investigations that normally take at least two days and require educated personnel. Here we offer a pre investigation to diagnose the sample as dangerous or not. In some cases, the spring water would not need to be analyzed, which was determined in 1 h by this on-chip electrical measurement. However, our test cannot be a gold standard due to the fact that our micro fabricated device cannot detect what is inside the sample. The test results can only claim whether there is potentially something dangerous in the sample with regards to impedance peaks. The suspected particles can be either solid particles, non-dangerous living species or pathogens, which can be revealed by further microbiological investigation. However, our test can decrease cost and time in analyzing water samples. For example, on-chip electrical measurement tests show that our plain water sample doesn't have any dangerous particles, which removes the need to send the sample for microbiological analysis. This method does not only reduce the cost; it also saves time with completion in 1 h. The electronic and pumping components of the device have a chance of being

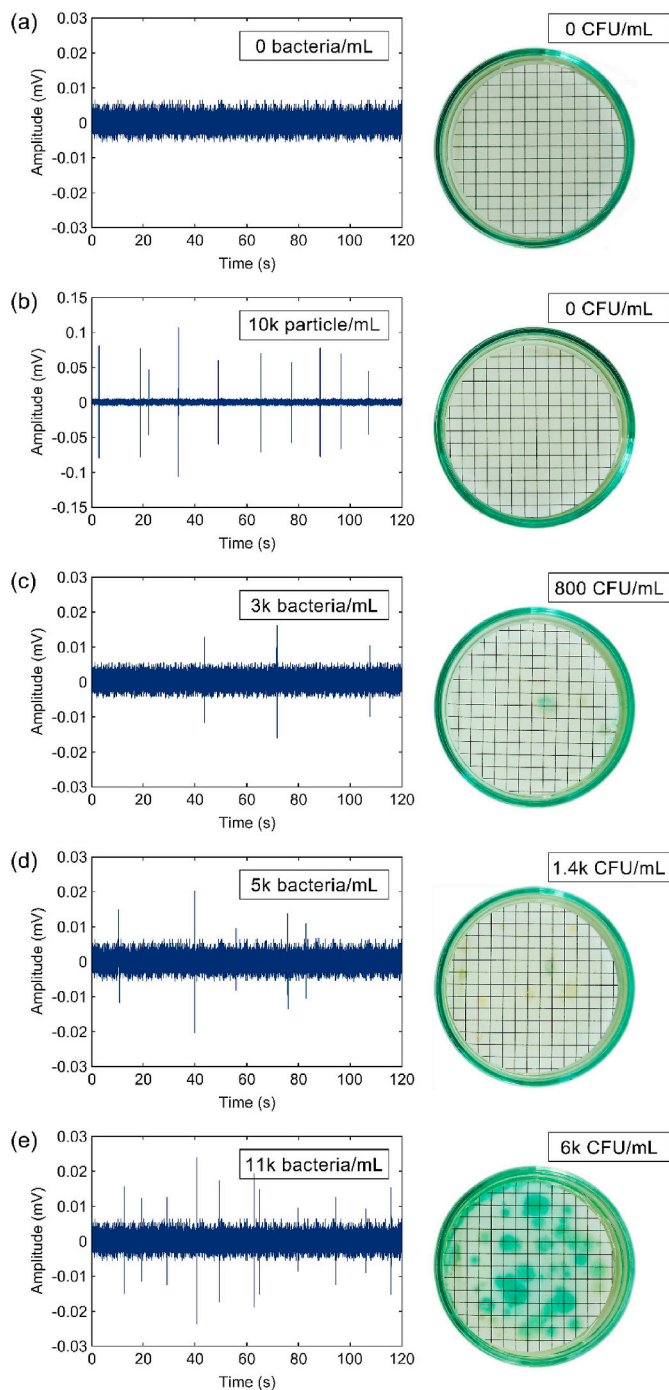


Fig. 7. Comparative results of both methods where the real output data of the electrical microfluidic measurement and the photographs of the microbiological assays are given for several cases: (a) the plain solution does not give either an electrical peak or any spot in the microbiological assay (b) the micro beads solution gives peaks in the electrical method while giving a negative result in the microbiological assay as expected (c) low contamination *P. aeruginosa* sample gives the least peaks for the electrical measurement in accordance with the microbiological analysis giving the least spots, (d) medium contaminated sample gives relatively higher peaks for the electrical measurement together with a microbiological assay greater than the low contamination sample, (e) highly contaminated sample outnumbered the other samples for the electrical measurement and a microbiological analysis with the highest number of peaks and spots.

miniaturized, which make it a good candidate for a hand-held POC (point of care) device for testing the water samples at source in minutes. In addition, our device does not need educated operators and offers a test that can be done by anybody who is capable of taking a water sample.

Author contribution

Ismail Bilican: Formal analysis, Methodology, Investigation, Writing - original draft, Writing - review & editing, Visualization, Tolga Bahadır: Formal analysis, Methodology, Investigation, Writing - original draft, Kemal Bilgin: Resources, Writing - original draft, Mustafa Tahsin Guler: Formal analysis, Methodology, Investigation, Writing - original draft, Writing - review & editing, Supervision

Declaration of competing interest

The authors declare that they have no known competing financial interests or personal relationships that could have appeared to influence the work reported in this paper.

Acknowledgements

The authors would like to thank Cabir Cagri Gence for his comments on the manuscript. This study was financially supported by Aksaray University (BAP Project: 2018–047).

Appendix A. Supplementary data

Supplementary data to this article can be found online at <https://doi.org/10.1016/j.talanta.2020.121293>.

References

- [1] H.E. Ayliffe, A.B. Frazier, R.D. Rabbitt, Electric impedance spectroscopy using microchannels with integrated metal electrodes, *IEEE J. Microelectromechanical Syst.* 8 (1999) 50–57, <https://doi.org/10.1109/84.749402>.
- [2] D. Holmes, H. Morgan, Single cell impedance cytometry for identification and counting of CD4 T-cells in human blood using impedance labels, *Anal. Chem.* 82 (2010) 1455–1461, <https://doi.org/10.1021/ac902568p>.
- [3] S. Zheng, M.S. Nandra, C.Y. Shih, W. Li, Y.C. Tai, Resonance impedance sensing of human blood cells, *Sensors Actuators, A Phys.* 145–146 (2008) 29–36, <https://doi.org/10.1016/j.sna.2007.10.047>.
- [4] G. Mernier, N. Piacentini, R. Tornay, N. Buffi, P. Renaud, Cell viability assessment by flow cytometry using yeast as cell model, *Sensor. Actuator. B Chem.* 154 (2011) 160–163, <https://doi.org/10.1016/j.snb.2009.11.066>.
- [5] Y. Zhou, S. Basu, E. Laue, A.A. Seshia, Single cell studies of mouse embryonic stem cell (mESC) differentiation by electrical impedance measurements in a microfluidic device, *Biosens. Bioelectron.* 81 (2016) 249–258, <https://doi.org/10.1016/j.bios.2016.02.069>.
- [6] E. Rollo, E. Tenaglia, R. Genolet, E. Bianchi, A. Harari, G. Coukos, C. Guiducci, Label-free identification of activated T lymphocytes through tridimensional micro-sensors on chip, *Biosens. Bioelectron.* 94 (2017) 193–199, <https://doi.org/10.1016/j.bios.2017.02.047>.
- [7] I. Bilican, M.T. Guler, M. Serhatlioglu, T. Kirindi, C. Elbuken, Focusing-free impedimetric differentiation of red blood cells and leukemia cells: a system optimization, *Sensor. Actuator. B Chem.* 307 (2020) 127531, <https://doi.org/10.1016/j.snb.2019.127531>.
- [8] J. Ko, E. Carpenter, D. Issadore, Detection and isolation of circulating exosomes and microvesicles for cancer monitoring and diagnostics using micro-/nano-based devices, *Analyst* 141 (2016) 450–460, <https://doi.org/10.1039/c5an01610j>.
- [9] A. Saateh, A. Kalantarifard, O.T. Celik, M. Asghari, M. Serhatlioglu, C. Elbuken, Real-time impedimetric droplet measurement (IDM), *Lab Chip* 19 (2019) 3815–3824, <https://doi.org/10.1039/c9lc00641a>.
- [10] S. Murali, X. Xia, A.V. Jagtiani, J. Carletta, J. Zhe, Capacitive Coulter counting: detection of metal wear particles in lubricant using a microfluidic device, *Smart Mater. Struct.* 18 (2009), <https://doi.org/10.1088/0964-1726/18/3/037001>.
- [11] Q. Liu, X. Zhang, Y. Yao, W. Jing, S. Liu, G. Sui, A novel microfluidic module for rapid detection of airborne and waterborne pathogens, *Sensor. Actuator. B Chem.* 258 (2018) 1138–1145, <https://doi.org/10.1016/j.snb.2017.11.113>.

- [12] R.T. Noble, S.B. Weisberg, A review of technologies for rapid detection of bacteria in recreational waters, *J. Water Health* 3 (2005) 381–392, <https://doi.org/10.2166/wh.2005.051>.
- [13] C. Bernabini, D. Holmes, H. Morgan, Micro-impedance cytometry for detection and analysis of micron-sized particles and bacteria, *Lab Chip* 11 (2011) 407–412, <https://doi.org/10.1039/c0lc00099j>.
- [14] N. Haandbæk, O. With, S.C. Bürgel, F. Heer, A. Hierlemann, Resonance-enhanced microfluidic impedance cytometer for detection of single bacteria, *Lab Chip* 14 (2014) 3313–3324, <https://doi.org/10.1039/c4lc00576g>.
- [15] S. Gawad, L. Schild, P. Renaud, Micromachined impedance spectroscopy flow cytometer for cell analysis and particle sizing, *Lab Chip* 1 (2001) 76–82, <https://doi.org/10.1039/b103933b>.
- [16] D.A. Boehm, P.A. Gottlieb, S.Z. Hua, On-chip microfluidic biosensor for bacterial detection and identification, *Sensor. Actuator. B Chem.* 126 (2007) 508–514, <https://doi.org/10.1016/j.snb.2007.03.043>.
- [17] S. Brosel-Oliu, R. Ferreira, N. Uria, N. Abramova, R. Gargallo, F.X. Muñoz-Pascual, A. Bratov, Novel impedimetric aptasensor for label-free detection of *Escherichia coli* O157:H7, *Sensor. Actuator. B Chem.* 255 (2018) 2988–2995, <https://doi.org/10.1016/j.snb.2017.09.121>.
- [18] M.S. Mannoos, S. Zhang, A.J. Link, M.C. McAlpine, Electrical detection of pathogenic bacteria via immobilized antimicrobial peptides, *Proc. Natl. Acad. Sci. U.S.A.* 107 (2010), <https://doi.org/10.1073/pnas.1008768107> 19207–19212.
- [19] L. Yang, R. Bashir, Electrical/electrochemical impedance for rapid detection of foodborne pathogenic bacteria, *Biotechnol. Adv.* 26 (2008) 135–150, <https://doi.org/10.1016/j.biotechadv.2007.10.003>.
- [20] H. Park, D. Kim, K.S. Yun, Single-cell manipulation on microfluidic chip by dielectrophoretic actuation and impedance detection, *Sensor. Actuator. B Chem.* 150 (2010) 167–173, <https://doi.org/10.1016/j.snb.2010.07.020>.
- [21] H. Young, R. Boris, Flow-through micro-electroporation chip for high efficiency single-cell genetic manipulation, *Sensors Actuators, A Phys.* 104 (2003) 205–212, [https://doi.org/10.1016/S0924-4247\(03\)00050-5](https://doi.org/10.1016/S0924-4247(03)00050-5).
- [22] T. Guo, Y. Wei, C. Xu, B.R. Watts, Z. Zhang, Q. Fang, H. Zhang, P.R. Selvaganapathy, M.J. Deen, Counting of *Escherichia coli* by a microflow cytometer based on a photonic-microfluidic integrated device, *Electrophoresis* 36 (2015) 298–304, <https://doi.org/10.1002/elps.201400211>.
- [23] I. Bernat, J.J. Gonzalez-Murillo, L. Fonseca, M. Moreno, A. Romano-Rodriguez, Optical particle detection in liquid suspensions with a hybrid integrated microsystem, *Sensors Actuators, A Phys.* 247 (2016) 629–640, <https://doi.org/10.1016/j.sna.2016.06.003>.
- [24] M. Xu, R. Wang, Y. Li, Electrochemical biosensors for rapid detection of *Escherichia coli* O157:H7, *Talanta* 162 (2017) 511–522, <https://doi.org/10.1016/j.talanta.2016.10.050>.
- [25] L. Wang, X. Huo, W. Qi, Z. Xia, Y. Li, J. Lin, Rapid and sensitive detection of *Salmonella Typhimurium* using nickel nanowire bridge for electrochemical impedance amplification, *Talanta* 211 (2020) 120715, <https://doi.org/10.1016/j.talanta.2020.120715>.
- [26] V. Koubová, E. Brynda, L. Karasová, J. Škvor, J. Homola, J. Dostálek, P. Tobiška, J. Rošický, Detection of foodborne pathogens using surface plasmon resonance biosensors, *Sensor. Actuator. B Chem.* 74 (2001) 100–105, [https://doi.org/10.1016/S0925-4005\(00\)00717-6](https://doi.org/10.1016/S0925-4005(00)00717-6).
- [27] E. Yilmaz, D. Majidi, E. Ozgur, A. Denizli, Whole cell imprinting based *Escherichia coli* sensors: a study for SPR and QCM, *Sensor. Actuator. B Chem.* 209 (2015) 714–721, <https://doi.org/10.1016/j.snb.2014.12.032>.
- [28] N.V. Lavrik, M.J. Sepaniak, P.G. Datskos, Cantilever transducers as a platform for chemical and biological sensors, *Rev. Sci. Instrum.* 75 (2004) 2229–2253, <https://doi.org/10.1063/1.1763252>.
- [29] K. Niitsu, S. Ota, K. Gamo, H. Kondo, M. Hori, K. Nakazato, Development of microelectrode arrays using electroless plating for CMOS-based direct counting of bacterial and HeLa cells, *IEEE Trans. Biomed. Circuits Syst.* 9 (2015) 607–619, <https://doi.org/10.1109/TBCAS.2015.2479656>.
- [30] S. Etcheverry, A. Faridi, H. Ramachandriaiah, T. Kumar, W. Margulis, F. Laurell, A. Russon, High performance micro-flow cytometer based on optical fibres, *Sci. Rep.* 7 (2017) 1–8, <https://doi.org/10.1038/s41598-017-05843-7>.
- [31] A. Golberg, G. Linshiz, I. Kravets, N. Stawski, N.J. Hillson, M.L. Yarmush, R.S. Marks, T. Konry, Cloud-enabled microscopy and droplet microfluidic platform for specific detection of *Escherichia coli* in water, *PLoS One* 9 (2014) e86341, <https://doi.org/10.1371/journal.pone.0086341>.
- [32] J. Kudr, O. Zitka, M. Klimanek, R. Vrba, V. Adam, Microfluidic electrochemical devices for pollution analysis—A review, *Sensor. Actuator. B Chem.* 246 (2017) 578–590, <https://doi.org/10.1016/j.snb.2017.02.052>.
- [33] A. Giorgini, S. Avino, P. Malara, R. Zullo, P. De Natale, K. Mrkvová, J. Homola, G. Gagliardi, Surface-plasmon optical-heterodyne clock biosensor, *Sensor. Actuator. B Chem.* 273 (2018) 336–341, <https://doi.org/10.1016/j.snb.2018.06.028>.
- [34] B.J. Yakes, J. Buijs, C.T. Elliott, K. Campbell, Surface plasmon resonance biosensing: approaches for screening and characterising antibodies for food diagnostics, *Talanta* 156–157 (2016) 55–63, <https://doi.org/10.1016/j.talanta.2016.05.008>.
- [35] K. Nieradka, K. Kapczyńska, J. Rybka, T. Lipiński, P. Grabiec, M. Skowicki, T. Gotszalk, Microcantilever array biosensors for detection and recognition of Gram-negative bacterial endotoxins, *Sensor. Actuator. B Chem.* 198 (2014) 114–124, <https://doi.org/10.1016/j.snb.2014.03.023>.
- [36] A. Salman, H. Carney, S. Bateson, Z. Ali, Shunting microfluidic PCR device for rapid bacterial detection, *Talanta* 207 (2020) 120303, <https://doi.org/10.1016/j.talanta.2019.120303>.
- [37] L.X. Wang, J.J. Fu, Y. Zhou, G. Chen, C. Fang, Z.S. Lu, L. Yu, On-chip RT-LAMP and colorimetric detection of the prostate cancer 3 biomarker with an integrated thermal and imaging box, *Talanta* 208 (2020) 120407, <https://doi.org/10.1016/j.talanta.2019.120407>.
- [38] G. Czilwik, T. Messinger, O. Strohmeier, S. Wadle, F. Von Stetten, N. Paust, G. Roth, R. Zengerle, P. Saarinen, J. Niittymäki, K. McAllister, O. Sheils, J. O’Leary, D. Mark, Rapid and fully automated bacterial pathogen detection on a centrifugal-microfluidic LabDisk using highly sensitive nested PCR with integrated sample preparation, *Lab Chip* 15 (2015) 3749–3759, <https://doi.org/10.1039/c5lc00591d>.
- [39] M.T. Guler, I. Bilican, Capacitive detection of single bacterium from drinking water with a detailed investigation of electrical flow cytometry, *Sensors Actuators, A Phys.* 269 (2018) 454–463, <https://doi.org/10.1016/j.sna.2017.12.008>.
- [40] B. Ramaswamy, Y.T.T. Yeh, S.Y. Zheng, Microfluidic device and system for point-of-care blood coagulation measurement based on electrical impedance sensing, *Sensor. Actuator. B Chem.* 180 (2013) 21–27, <https://doi.org/10.1016/j.snb.2011.11.031>.
- [41] P.J.R. Roche, M. Najih, S.S. Lee, L.K. Beitel, M.L. Carnevale, M. Paliouras, A.G. Kirk, M.A. Trifiro, Real time plasmonic qPCR: how fast is ultra-fast? 30 cycles in 54 seconds, *Analyst* 142 (2017) 1746–1755, <https://doi.org/10.1039/c7an00304h>.
- [42] M.T. Guler, Z. Isiksacan, M. Serhatlioglu, C. Elbuken, Self-powered disposable prothrombin time measurement device with an integrated effervescent pump, *Sensor. Actuator. B Chem.* 273 (2018) 350–357, <https://doi.org/10.1016/j.snb.2018.06.042>.
- [43] B. Zhao, X. Cui, W. Ren, F. Xu, M. Liu, Z.G. Ye, A controllable and integrated pump-enabled microfluidic chip and its application in droplets generating, *Sci. Rep.* 7 (2017) 1–8, <https://doi.org/10.1038/s41598-017-10785-1>.
- [44] B. Jose, P. McCluskey, N. Gilmartin, M. Somers, D. Kenny, A.J. Ricco, N.J. Kent, L. Basabe-Desmonts, Self-Powered microfluidic device for rapid assay of antiplatelet drugs, *Langmuir* 32 (2016) 2820–2828, <https://doi.org/10.1021/acs.langmuir.5b03540>.
- [45] F. Dal Dosso, T. Kokalj, J. Belotserkovsky, D. Spasic, J. Lammertyn, Self-powered infusion microfluidic pump for ex vivo drug delivery, *Biomed. Microdevices* 20 (2018) 1–11, <https://doi.org/10.1007/s10544-018-0289-1>.
- [46] C. Barbosa, T. Dong, Modelling and design of a capacitive touch sensor for urinary tract infection detection at the point-of-care, 2014 36th, *Annu. Int. Conf. IEEE Eng. Med. Biol. Soc. EMBC* 2014 (2014) 4995–4998, <https://doi.org/10.1109/EMBC.2014.6944746>.
- [47] H. Zhu, U. Sikora, A. Ozcan, Quantum dot enabled detection of *Escherichia coli* using a cell-phone, *Analyst* 137 (2012) 2541–2544, <https://doi.org/10.1039/c2an35071h>.
- [48] P.B. Lillehoj, M.-C. Huang, N. Truong, C.-M. Ho, Rapid electrochemical detection on amobile phone, *Lab Chip* 15 (2013) 2950–2955, <https://doi.org/10.1039/c2lc41193h>.
- [49] H. Guner, E. Ozgur, G. Kokturk, M. Celik, E. Esen, A.E. Topal, S. Ayas, Y. Uludag, C. Elbuken, A. Dana, A smartphone based surface plasmon resonance imaging (SPRI) platform for on-site biodetection, *Sensor. Actuator. B Chem.* 239 (2017) 571–577, <https://doi.org/10.1016/j.snb.2016.08.061>.